Raman effect and structure of YH_3 and YD_3 thin epitaxial films

H. Kierey,* M. Rode, A. Jacob, A. Borgschulte, and J. Schoenes
Institut für Halbleiterphysik and Optik, Technische Universität Braunschweig, Mendelssohnstrasse 3, D-38106 Braunschweig, Germany
(Received 19 September 2000; published 14 March 2001)

The first-order Raman spectra of YH_3 and YD_3 thin epitaxial films deposited on CaF_2 substrates have been studied in the temperature range from 4 to 300 K. Several rather broad Raman lines from YH_3 have been found. The linewidth becomes smaller with decreasing temperature and the lines are very distinct and sharp at 4 K. No indications for phase transitions are found. Isotopically exchanged samples give a clear indication that YH_3 is at the origin of the Raman lines. Polarization resolved measurements together with a factor group analysis for all suggested crystal structures of YH_3 reveals the number and the symmetry of the phonon modes. The number of observed A_1 modes is not compatible with a $P\bar{3}c1$ structure. Calculations of the angular dependence at different inclination angles result in predictions for characteristic intensity patterns for the suggested crystal structures. The measured angular intensity pattern show no indications for a $P\bar{3}c1$ structure. In measurements at different inclination angles new Raman lines appear, which points towards a $P6_3cm$ or $P6_3$ structure. Also the comparison of the energies of the lines in the Raman and in IR spectra promotes the picture of a noncentrosymmetric structure such as $P6_3cm$ or $P6_3$.

DOI: 10.1103/PhysRevB.63.134109 PACS number(s): 78.30.Hv, 63.20.Dj

I. INTRODUCTION

Since the discovery of their novel switchable optical properties the hydrides of yttrium and other rare-earth metals have been the subject of increasing research. The completely reversible transition from a shiny metal to a transparent insulator, which is achieved simply by hydrogenation of an Y film, offers a great potential both for practical applications and for basic investigations.

Generally it is believed, that in the hydrogenation process of an yttrium film three different phases are involved.[1] The starting point is the hexagonal closed packed structure of metallic Y, where hydrogen exists only in solid solution (α phase). Above a hydrogen content of $x=0.23$ in YH_x the α phase coexists with a fcc-based, still metallic β phase. In the region between $x=1.8$ and $x=2.1$ only the β phase is stable. If the hydrogen content is higher than $x=2.1$ a hexagonal γ phase starts to form, which is the only stable phase above $x=2.75$. A metal-insulator transition occurs for $x\approx 2.75$, which is, however, not believed to be driven by the structural phase transition.[1]

So far, a reliable theoretical model of this metal-insulator transition is not available. One of the prerequisites for the development of such a theoretical description would be the knowledge of the crystal structure of the YH_3 films. Whereas the structures of the α and β phase are known, this is not the case for YH_3. Several different structures for YH_3 have been proposed from different groups: From early x-ray diffraction experiments a simple hcp structure was inferred. Neutron powder diffraction studies[2,3] found, that the symmetry is more likely $P\bar{3}c1$. Later the same authors argued, that a $P6_3cm$ structure is also compatible with their experimental data.[4,5] LDA band structure calculations from another group claimed that the structure with the lowest energy has $P6_3$ symmetry.[6,7] For the $P\bar{3}c1$ structure this group did not find an energy gap in YH_3. In neutron diffraction experiments YH_3 with $P6_3$ symmetry should exhibit additional diffraction peaks. Experiments with an epitaxial thin film of YH_3 on CaF_2 showed none of these additional features.[8]

In this paper we present measurements of the Raman effect in YH_3 and YD_3 films. Since the first order Raman lines allow a very precise determination of zone-center optical phonon energies, this gives reliable information for more realistic models and thus might help to come to better theoretical descriptions of this material. Moreover, because of the strong dependence of the number, intensity, and polarization of the Raman lines on the crystal structure of a material, it is possible to check whether or not a suggested crystal structure is compatible with the observations.

II. THEORY

The Raman and infrared activity of phonon branches depends only on their symmetries and general selection rules. Energy and momentum conservation limits the first order observation of phonons in Raman and infrared spectroscopy to the center of the Brillouin zone. Here all optical phonons are standing waves and the unit cells vibrate in phase. Therefore the number of phonon branches, their symmetry and the motion pattern of the atoms in the unit cell can be estimated with an analysis of the factor group of the unit cell only.[9–11] This calculation is performed in the first part of this section. With the information about the symmetry the polarization of the Raman lines and the angular dependence of the intensity is then derived in the second part. This enables the identification of the symmetry of the phonons in the Raman spectra.

A. Factor group analysis

For the factor group analysis (FGA) the space group and the site occupation of the material under investigation has to be known. This information is collected in Table I for the various structures proposed for YH_3 and in Table II for the other materials and phases of yttrium and hydrogen possibly present in the samples. This is necessary because all parts of

TABLE I. Input data for the FGA of YH_3.

Space group	No.	Schönflies	Atoms/unit cell	Site occupation[a]	Reference
$P6_3mmc$	194	D_{6h}^4	8	Y on $2c$, H on $2a+4f$	Simple hcp structure claimed earlier from x-ray diffraction
$P\bar{3}c1$	165	D_{3d}^4	24	Y on $6f$, H on $2a+4d+12g$	Derived from neutron diffraction experiments (Refs. 2, 3)
$P6_3cm$	185	C_{6v}^3	24	Y on $6c$, H on $6c+6c+4b+2a$	Also compatible with the neutron diffraction data (Refs. 4, 5)
$P6_3$	173	C_6^6	24	Y on $6c$, H on $6c+6c+2b+2b+2a$	Theoretical lowest-energy structure from LDA calculations (Refs. 6, 7)

[a]See, for example, the tables of Wyckoff positions on the Bilbao Crystallographic Server (Ref. 12).

the sample (substrate, film, cap layer, metallic Y, YH_2) might contribute to the signal and show their own specific Raman lines.

In the center of the Brillouin zone all normal coordinates can be classified according to the irreducible representations of the point group of the crystal. This is due to the fact, that all normal coordinates are mapped on themselves by the use of one of the symmetry operations of the symmetry group of the crystal and therefore form a basis of a (reducible) representation of this group.[10] With standard group theoretical methods the number and type of irreducible representations of the factor group can be calculated.[9]

The results for YH_3 are listed in Table III and for the other materials in Table IV. The possible structures of YH_3 can be divided into two groups: the $P6_3mmc$ and the $P\bar{3}c1$ structures have inversion symmetry, whereas $P6_3cm$ and $P6_3$ do not. In the first group all Raman active phonon modes are not infrared active and vice versa. In contrast, for the second group the A-like and the doubly degenerated E_1 phonons are both infrared and Raman active. This offers a possible way of distinguishing experimentally between the first and the second types of structures: if one can find phonons of the appropriate symmetry species at the same energy both in Raman and infrared spectra of YH_3, then there cannot exist a center of inversion symmetry and therefore one of the structures of the second group is the correct one. The number of phonon modes is the maximum number of observable lines. Some of the Raman lines might be too weak to be seen in the spectra and the difference in energy of others might be too small to separate them. However finding more lines in the spectra then allowed for a given structure, shows that the structure cannot be correct.

The analysis of the other materials shows, that there is only one Raman active line from pure Y and also only one from YH_2 and CaF_2. The Pd cap layer should not produce any lines. The lines from pure Y and CaF_2 are known[13] and are located at 88.5 and 322 cm^{-1}, respectively, while no Raman data on YH_2 exists to our knowledge.

B. Polarization of the Raman lines

With the knowledge of the symmetry species of the phonons for all structures, the polarization and the angular dependence of the intensity of the Raman lines can be calculated. The intensity I of a Raman line depends on the polarizations $\mathbf{e}_i$ and $\mathbf{e}_s$ of the incident and scattered light and the Raman tensor $R_{\sigma\rho}$ by

$$I \sim \left| \sum_{\rho,\sigma=x,y,z} e_i^{\sigma} R_{\sigma\rho} e_s^{\rho} \right|^2 .$$

The Raman tensors $R_{\sigma\rho}$ for all Raman active phonon symmetry species in all point groups are tabulated[9,10,14] and the relevant tensors for the different structures of YH_3 and for the other materials are collected in the Tables V and VI, respectively.

A given *scattering geometry* reduces the possible values of $\mathbf{e}_i$ and $\mathbf{e}_s$. According to Fig. 1 a 180°-backscattering configuration was used in our case. The scattered light always propagates back in the opposite direction of the incident light. The sample normal deviates from the beam direction by an angle ϕ, which was chosen to be 0° or 45° in our experiments. The sample could be rotated around its surface normal to study different directions in the crystal. Since the directions of the incident and the scattered beam are collinear we have two main configurations for the polarization vectors. If they are parallel to each other we denote this fact with $\parallel$ and if they are perpendicular with $\perp$. Experimentally the two cases are realized with a fixed polarizer in front of the en-

TABLE II. Input data for the FGA of metallic Y, YH_2, the Pd cap layer and the CaF_2 substrate.

Material	Space group	No.	Schönflies	Atoms/unit cell	Site occupation (Ref. 12)
Y hcp	$P6_3mmc$	194	D_{6h}^4	2	Y on $2c$
YH_2 fcc	$Fm\bar{3}m$	225	O_h^5	3	Y on $4a$, H on $8c$
CaF_2 fcc	$Fm\bar{3}m$	225	O_h^5	3	Ca on $4a$, F on $8c$
Pd fcc	$Fm\bar{3}m$	225	O_h^5	1	Pd on $4a$

TABLE III. Results of the FGA for YH_3. Translational components are subtracted.

Space group	Raman active modes	IR active modes	Silent modes
$P6_3mmc$	$A_{1g}+E_{1g}+2E_{2g}$	$2A_{2u}+2E_{2u}$	$2B_{1g}+2B_{2u}+2E_{2u}$
$P\bar{3}c1$	$5A_{1g}+12E_g$	$6A_{2u}+11E_u$	$5A_{1u}+7A_{2g}$
$P6_3cm$	$7A_1+11E_1+12E_2$	$7A_1+11E_1$	$4A_2+8B_1+4B_2$
$P6_3$	$11A+11E_1+12E_2$	$11A+11E_1$	$12B$

trance slit of the polychromator and a Soleil-Babinet compensator which changes the polarization of the light emitted by the laser.

The vectors $\mathbf{e}_i$ and $\mathbf{e}_s$ are defined in the coordinate system of the crystal. For the case of cubic systems the three basis vectors $\mathbf{x}_0,\mathbf{x}_1,\mathbf{x}_2$ are the same as the three cubic axes, for hexagonal and trigonal cases $\mathbf{x}_0$ is parallel to the a axis, $\mathbf{x}_1$ lies between the a axis and the $(a+b)$ axis and $\mathbf{x}_2$ is parallel to the c axis, which is the surface normal in our case. These axes are identical with the principal axes chosen by Nye.[15]

The results for the angular dependence of the intensities for the different structures are displayed in Table V. For all four possible configurations ($\phi=0°$, $\|$; $\phi=0°$, $\perp$; $\phi=45°$, $\|$; $\phi=45°$, $\perp$) the dependence on the angle of rotation of the sample about its surface normal is shown. Only within one line of the table is the axis scale kept constant.

It is possible to distinguish between the three types of symmetry species in all suggested structures of YH_3. *A*-like phonons are always $\|$ polarized, whereas E_1, E_2, and E_g phonons have an intensity in both polarization directions. Therefore no angular resolved measurements are necessary to identify *A*-like and *E*-like phonons. The E_g phonon in $P\bar{3}c1$ behaves somewhat like the E_2 phonon in the other structures, but shows a threefold pattern in the 45° configuration. However the ratio between the biggest and the smallest intensity might be close to one, if either the component c or d in the Raman tensor is close to zero. This corresponds to only very small differences between $P\bar{3}c1$ and other structures. To distinguish between E_1 and E_2 phonons it is necessary to change from the 0° orientation to the 45° orientation. If the intensity increases, it is an E_1 phonon, otherwise an E_2 phonon. If the structure is $P\bar{3}c1$, we should not observe an increase in intensity of *E*-like phonons and no new lines in the spectra as we go from the 0° orientation to the 45° orientation.

It should be noted, that because of the wide acceptance angle for the scattered light the selection rules in the experiment may not be as sharp as assumed in the calculation. Therefore, especially the E_1 phonons may appear in the 0° spectra, since their intensity is zero only exactly for scattered light traveling back along the direction of the surface normal.

The full dependence of the intensity on the inclination angle ϕ is displayed for all phonon species and for parallel polarization in Fig. 2. At 45° the intensity of the E_1-like phonons is maximal. Additionally it can be seen, that the three-fold pattern of the intensity of the E_g phonons in the $P\bar{3}c1$ structure is the normal case for every inclination angle except 0°.

III. EXPERIMENTAL DETAILS

A. Samples

Epitaxial yttrium films with a thickness of 200 nm were grown on (111) CaF_2 substrates at 700 °C as described in Refs. 16 and 17. The yttrium source was an *e*-gun evaporation system. The base pressure during the deposition was lower than 1×10^{-9} mbar. The thickness of the films was measured with a water-cooled quartz microbalance. To protect the yttrium films against oxidation, they were covered with a 20 nm Pd protective layer. This cap layer was deposited at room temperature to prevent any alloy formation with the yttrium. The quality of the yttrium epitaxial film was measured in situ by reflection high energy electron diffraction (RHEED). The RHEED patterns showed sharp streaks, Kikuchi lines and second order diffraction evidencing the high crystallinity of the yttrium layer.

B. Hydrogen loading

The samples were loaded with H_2 or D_2 and measured in a variable temperature He cryostat. The cryostat was operated with $\approx$20 mbar H_2 or D_2 as contact gas for measurements above 70 K and with He below that temperature. Some room temperature measurements were performed at a hydrogen pressure of 1 bar to ensure a maximum loading of the sample. The purity of H_2 and D_2 was 99.999 and 99.7 %, respectively.

TABLE IV. Results of the FGA for metallic Y, YH_2, Pd, and CaF_2. Translational components are subtracted.

Material	Raman active modes	IR active modes	Silent modes	Remarks
Y hcp	E_{2g}		B_{1g}	Only one Raman line (Ref. 13) at 88.5 cm^{-1}
YH_2 fcc	F_{2g}	F_{1u}		Only one Raman line, but not in literature
CaF_2 fcc	F_{2g}	F_{1u}		Only one Raman line at 322 cm^{-1}
Pd fcc				No Raman or IR active phonons

TABLE V. Raman tensors and angular dependence of the intensity of the scattered light for the Raman active phonon modes of YH_3. The scattering geometry is 180° backscattering along the *c* axis (0°) or with an angle of about 45° to the *c* axis according to Fig. 1. ∥ and ⊥ refer to the position of the analyzer parallel and perpendicular to the laser polarization, respectively. The angular dependence is calculated for a rotation of the sample about its own *c* axis.

Symmetry	Raman tensors[9]	Intensity 0° ∥	Intensity 0° ⊥	Intensity 45° ∥	Intensity 45° ⊥
$P6_3mmc$	$A_{1g}: \begin{pmatrix} a & 0 & 0 \\ 0 & a & 0 \\ 0 & 0 & b \end{pmatrix}$				
	$E_{1g}: \begin{pmatrix} 0 & 0 & 0 \\ 0 & 0 & c \\ 0 & c & 0 \end{pmatrix}, \begin{pmatrix} 0 & 0 & -c \\ 0 & 0 & 0 \\ -c & 0 & 0 \end{pmatrix}$				
	$E_{2g}: \begin{pmatrix} 0 & d & 0 \\ d & 0 & 0 \\ 0 & 0 & 0 \end{pmatrix}, \begin{pmatrix} d & 0 & 0 \\ 0 & -d & 0 \\ 0 & 0 & 0 \end{pmatrix}$				
$P\bar{3}c1$	$A_{1g}: \begin{pmatrix} a & 0 & 0 \\ 0 & a & 0 \\ 0 & 0 & b \end{pmatrix}$				
	$E_g: \begin{pmatrix} c & 0 & 0 \\ 0 & -c & d \\ 0 & d & 0 \end{pmatrix}, \begin{pmatrix} 0 & -c & -d \\ -c & 0 & 0 \\ -d & 0 & 0 \end{pmatrix}$				
$P6_3cm$	$A_1: \begin{pmatrix} a & 0 & 0 \\ 0 & a & 0 \\ 0 & 0 & b \end{pmatrix}$				
	$E_1: \begin{pmatrix} 0 & 0 & 0 \\ 0 & 0 & c \\ 0 & c & 0 \end{pmatrix}, \begin{pmatrix} 0 & 0 & -c \\ 0 & 0 & 0 \\ -c & 0 & 0 \end{pmatrix}$				
	$E_2: \begin{pmatrix} 0 & d & 0 \\ d & 0 & 0 \\ 0 & 0 & 0 \end{pmatrix}, \begin{pmatrix} d & 0 & 0 \\ 0 & -d & 0 \\ 0 & 0 & 0 \end{pmatrix}$				
$P6_3$	$A: \begin{pmatrix} a & 0 & 0 \\ 0 & a & 0 \\ 0 & 0 & b \end{pmatrix}$				
	$E_1: \begin{pmatrix} 0 & 0 & c \\ 0 & 0 & d \\ c & d & 0 \end{pmatrix}, \begin{pmatrix} 0 & 0 & -d \\ 0 & 0 & c \\ -d & c & 0 \end{pmatrix}$				
	$E_2: \begin{pmatrix} e & f & 0 \\ f & -e & 0 \\ 0 & 0 & 0 \end{pmatrix}, \begin{pmatrix} f & -e & 0 \\ -e & -f & 0 \\ 0 & 0 & 0 \end{pmatrix}$				

C. Raman spectrometer

The Raman spectra were recorded with a homemade Raman spectrometer, operating with a triple grating polychromator and a liquid N_2 cooled scientific CCD camera. As excitation radiation the 514.5 nm line of an Ar^+ laser was used. The laser light was filtered using a 2 nm FWHM interference filter to remove residual plasma lines and then focused onto the sample with a cylindrical lens. The laser power was 600 mW for all measurements, but due to losses in the interference filter only ≈50% reached the sample. To obtain the maximal intensity of the weak Raman lines all samples were measured through the transparent CaF_2 sub-

TABLE VI. Raman tensors and angular dependence for the Raman active phonon modes of Y, YH_2, and CaF_2. The scattering geometry is 180° backscattering along the *c* axis for Y and along the [111] direction for YH_2 and CaF_2.

Material	Symmetry	Raman tensors[9]	Intensity 0° ∥	Intensity 0° ⊥	Intensity 45° ∥	Intensity 45° ⊥
Y hcp	$P6_3mmc$	$E_{2g}: \begin{pmatrix} 0 & d & 0 \\ d & 0 & 0 \\ 0 & 0 & 0 \end{pmatrix}, \begin{pmatrix} d & 0 & 0 \\ 0 & -d & 0 \\ 0 & 0 & 0 \end{pmatrix}$				
CaF_2, YH_2	$Fm\bar{3}m$	$F_{2g}: \begin{pmatrix} 0 & 0 & 0 \\ 0 & 0 & d \\ 0 & d & 0 \end{pmatrix}, \begin{pmatrix} 0 & 0 & d \\ 0 & 0 & 0 \\ d & 0 & 0 \end{pmatrix}, \begin{pmatrix} 0 & d & 0 \\ d & 0 & 0 \\ 0 & 0 & 0 \end{pmatrix}$				

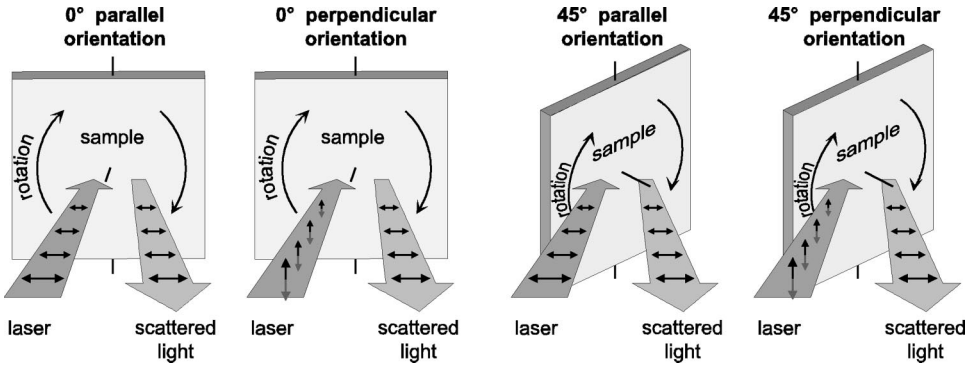

FIG. 1. Scattering configurations for the calculation of the angular dependence of the intensity. In all four configurations 180° backscattering is realized. For the angular dependence only the sample is rotated about an axis perpendicular to the surface.

strate from the back side. This avoided losses due to absorption in the Pd cap layer, which would have to be passed twice by the light—once by the laser and once by the scattered light. The spectrometer was calibrated with an Ar spectral lamp and high precision spectral line data from NIST (Ref. 18) to achieve a very accurate calibration. In our case an accuracy of better than ± 1 cm^{-1} was achieved. The usual natural line width of the spectrometer was about 6 cm^{-1} FWHM. For polarization resolved measurements, the direction of the laser polarization was rotated with a Soleil-Babinet compensator. The direction of the analyzer in front of the polychromator was kept constant, since the polychromator itself showed a strong polarization dependence of its grating efficiency.

D. Scattering geometry

For all measurements a 180°-backscattering geometry was used as indicated in Fig. 1. Since the crystallinity of the samples is very good, one can assume that for an angle of incidence of 0° the light propagates along the *c* axis of the hexagonal structure and for 45° the vector of incidence lies on a cone around the *c* axis. However, due to the wide acceptance angle (35°) for the collected scattered light the selection rules may not be as sharp as calculated in Sec. II, and some forbidden components may appear in the spectra. In order to achieve an angle of 45° between the *c* axis and the propagation direction of the light inside the sample, it is necessary to know the refractive index of YH_3 at the laser wavelength. The optical constants were measured by Lee *et al.*[19] for the infrared and visible range. From these data the refractive index can be estimated to be approximately 1.2 for a wavelength of 515 nm. Therefore an angle of incidence of about 60° is necessary outside the sample, to achieve an inclination of 45° to the *c* axis inside the sample.

E. Raman lines from H_2 or D_2 gas and plasma lines

To determine the origin of the observed Raman lines, their spectral positions were compared with the known position of laser plasma excitation lines.[20] Since some of the measurements were performed in an H_2 or D_2 atmosphere also rotational Raman lines from the molecular gases appear in the spectra. These lines can easily be identified by their

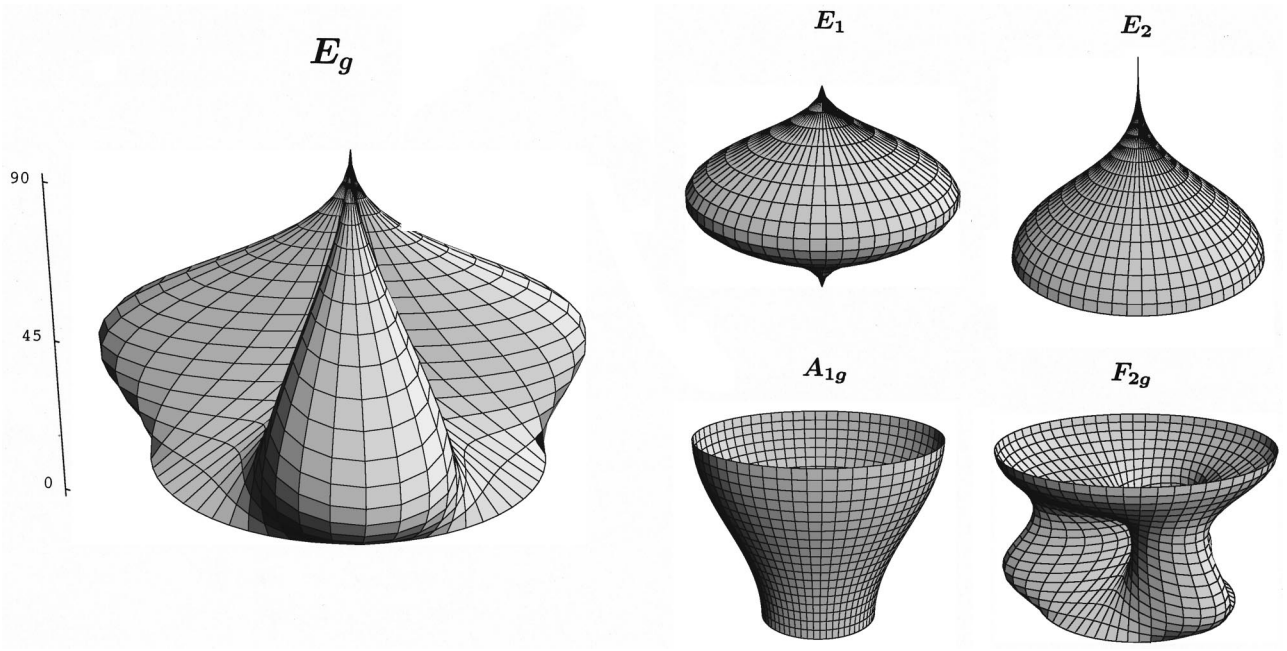

FIG. 2. Full angular dependence of the intensity for the five different symmetry species of Tables V and VI in parallel polarization. The angle ϕ is varied between 0° and 90° and the sample is rotated about its surface normal.

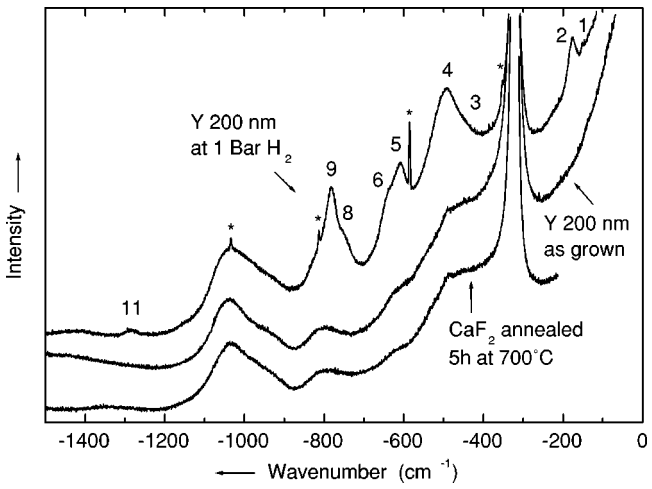

FIG. 3. Comparison of the Raman spectra for an annealed CaF_2 substrate, an as-grown 200 nm Y film capped with 20 nm of Pd and the film loaded with 1 bar of H_2 at room temperature. Rotational Raman lines from the H_2 atmosphere are visible in the spectra as sharp peaks and are marked with an asterisk. The numbers indicate the peaks according to Table VII.

very narrow spectral width. The energies are known from literature.[21] If H_2 is replaced by D_2 the energies are not shifted by the factor $1/\sqrt{2}$ as in the case of vibrational Raman lines from phonons or molecular vibrations, but by a factor of $\frac{1}{2}$. This is due to the quantization of the molecular rotational energy $E_r = j(j+1)\hbar^2/2\Theta$, where $\Theta = 2m_H r_H^2$ and j is even for *para*-H_2 and odd for *ortho*-H_2. For rotational transitions in homonuclear molecules Δj is even and the lines are equidistant in energy with a distance of $\Delta E = 2\hbar^2/\Theta$. However, if both *ortho*-and *para*-H_2 are present (as is the case here), lines are observed at a spacing of $\Delta E = \hbar^2/\Theta$ because the lines of the two species are interspaced. If hydrogen is replaced by deuterium the mass $m_D = 2m_H$ is doubled and the energy is divided by 2. Small deviations from this rule are due to centrifugal forces, which tend to increase the interatomic distance $2r_H$ and therefore lower the energy.

IV. RESULTS AND DISCUSSION

Our measurements showed no Raman lines at energies above 1400 cm^{-1}. Also from measurements of the phonon density of states with inelastic neutron scattering[2,22] it is known that all phonons have energies below 1400 cm^{-1}. Therefore in the following presentation of the experimental results the spectral range is limited to 0–1500 cm^{-1}.

A. Room temperature spectra

Figure 3 shows the room temperature Raman spectra of a pure CaF_2 substrate, an as-grown Y film and the same film after 1 h loading with H_2 at 1 bar. For this comparison a substrate was used, which was cleaned and annealed at 700 °C for 5 h in a similar manner as the substrates used for the growth of the Y film. The main feature in all three spectra is the CaF_2 line at 322 cm^{-1}. Some additional small and broad lines already appear in the spectrum of the substrate. These lines are very weak or even not present in normal CaF_2 crystals and are likely due to defects and especially empty fluorine sites formed during the annealing process.[23] The Y film itself did not show any new peaks. When the film was loaded several new lines arose, which are labeled by numbers in Fig. 3. The numbering of the peaks is held consistent throughout all spectra. Therefore, not all numbers appear in Fig. 3. The energies for the lines are collected in Table VII. Some very sharp peaks are rotational Raman lines from H_2 gas and are marked with an asterisk. The Raman lines from YH_3 are rather broad at room temperature and many of the lines are not clearly separated, as in the case for lines 3 and 4; 5 and 6; and 8 and 9. The energies were estimated by fitting the spectrum with Lorentzians. Therefore the accuracy is not as good for the smaller peaks in proximity of the stronger peaks as for the strong peaks themselves. The accuracy is given in Table VII for all lines. In the H-loaded films also a line at 92.6 cm^{-1} appears as shown in Fig. 4. The sidelobe of the laser line has been subtracted in Fig. 4 to enhance the visibility. This line is the known[13] Raman line of metallic Y, which is normally found at 88.5 cm^{-1}. The difference in energy can be explained by strain, if

TABLE VII. Spectral position and accuracy of the Raman lines for room temperature and 4 K and for the IR lines at 77 K. Line 7 is visible in Raman spectra only if the angle of incidence is 45°.

No.	Phonon mode	Peak position for H_2 (cm^{-1}) 300 K	Peak position for H_2 (cm^{-1}) 4 K	Peak position for D_2 (cm^{-1}) 300 K	Peak position for D_2 (cm^{-1}) 4 K	IR for H_2 (cm^{-1}) 77 K
1	E	153±3	153±2	153±3	154±2	
2	A_1	178±1	188±1	184±5	187±1	
3	A_1	466±10	443±2			
4	A_1	499±10	488±2		367±2	
5	A_1	610±3	620±2	442±3	451±2	617
6	A_1	644±5	655±2	467±10	477±5	
7	E_1		726±2		531±10	724
8	E_2	751±5	760±2	541±10	551±5	
9	A_1	784±3	784±2	563±3	563±10	770
10	E_1	899±10	906±10	617±10	630±10	911
11	E_1	1283±3	1300±2	924±3	938±10	1290

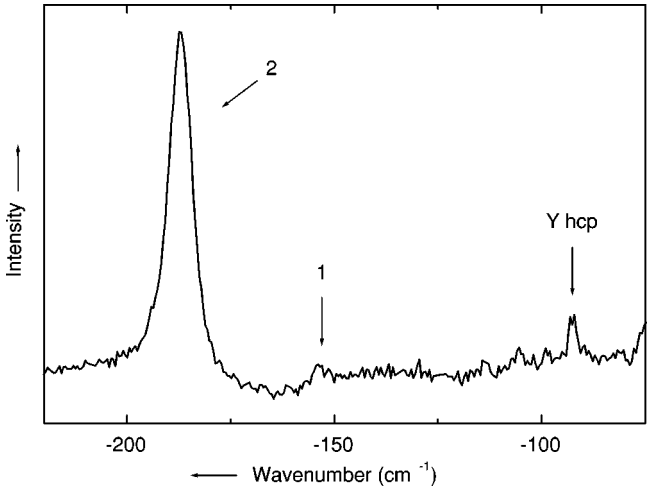

FIG. 4. The known Raman line from metallic Y in a loaded YH_3 film. The sidelobe of the laser line is subtracted here to enhance the visibility.

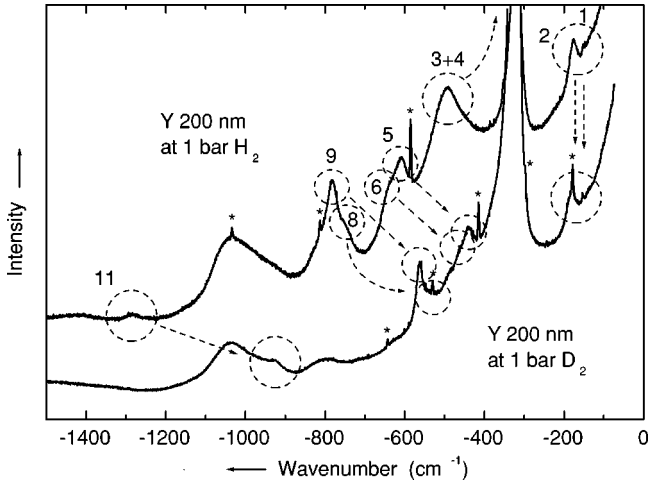

FIG. 5. Comparison of the room temperature Raman spectra for a loading with H_2 and D_2. Rotational Raman lines from the H_2 or D_2 gas atmosphere are visible in the spectra as sharp peaks and are marked with an asterisk.

this line originates from small Y clusters embedded in an oxide and therefore unable to hydride. The number of observed Raman lines shows, that the simple hcp structure with a small unit cell and $P6_3mmc$ symmetry cannot be correct. In this structure only four Raman lines are allowed.

B. Isotope-exchange measurements

To ensure that the origin of the Raman lines is the hydride and not impurities (for example of fluorines[23] YF_x) in the films, and to find out the contribution of Y and H to the vibrations we measured isotopically substituted samples. For this purpose an Y film was loaded in 1 bar of D_2. The resulting spectra are compared with those for hydrogen loaded samples in Fig. 5. From the theory one would expect a shift of vibrational Raman lines by a factor of $1/\sqrt{2}$ because of the double mass of deuterium compared to hydrogen. The experiment shows indeed a dramatic change in the spectral positions of the lines. From the ratios of the intensities the lines can easily be related to those of a hydrogenated sample. This is also shown in Fig. 5. Only lines 3 and 4 are hidden under the strong CaF_2 line. The lines designated with 1 and 2 stay nearly at the same position. This shows that their origin is a vibration of Y atoms in the YH_3 phase. The shift from the original position[13] of 88.5 cm^{-1} for the E_2 phonon in hexagonal Y is remarkably large, but can be explained by the big change in the size of the unit cell[3] of YH_3 compared to pure Y. The energies of the Raman lines of the YD_3 sample are collected together with their errors in Table VII. Some very sharp peaks in the spectra are again rotational Raman lines from H_2 or D_2. In contrast to the vibrational lines they are shifted by the factor $\frac{1}{2}$ as explained in Sec. III E. These lines are marked by an asterisk in Fig. 5.

C. Low-temperature spectra

Since all Raman lines from YH_3 are rather broad at room temperature, low temperature measurements at 77 K and at 4 K and temperature resolved measurements have been performed. A comparison of the spectra for 300, 77, and 4 K can be seen in Fig. 6. Many new lines are visible at low temperature due to their decreased linewidth and increased intensity. All lines marked with numbers are also present in spectra of YD_3 at low temperature (not shown). Sharp peaks at 1120, 1160, 1021, 1002, and 990 cm^{-1} originate from the substrate and are visible only at low temperature. The energies for 4 K are again collected in Table VII together with the errors estimated from the fit process. The smaller width of the peaks allows the determination of the energies at 4 K with better accuracy than at 300 K. The difference between the spectra taken at 77 and 4 K is not very large. Directly in the laser focus the temperature is expected to be somewhat higher than 4 K. It is difficult to determine the exact temperature, since the usual method, the measurement of the intensity ratio of anti-Stokes and Stokes lines, cannot be used below 70 K due to the exponential decrease of the anti-

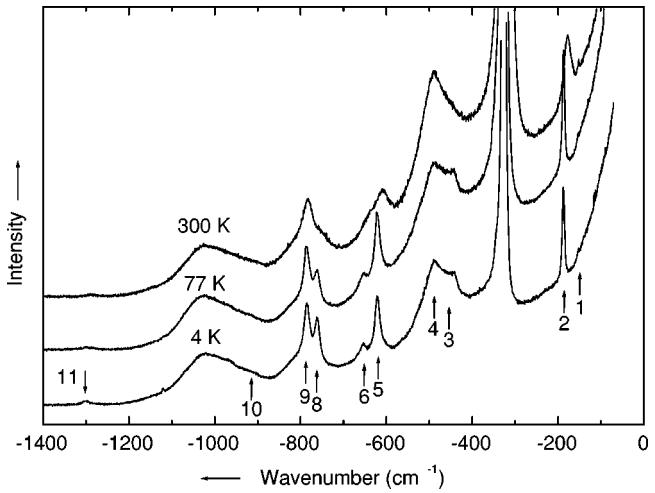

FIG. 6. Raman spectra of an YH_3 film taken at room temperature, at 77 and at 4 K. The numbers indicate the peaks according to Table VII.

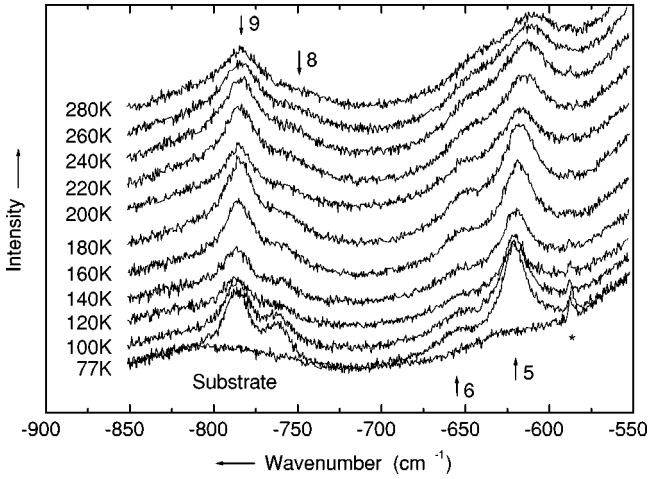

FIG. 7. Evolution with temperature of the Raman lines of YH_3 in the region around 600 and 800 cm^{-1} and a Raman spectrum of a pure CaF_2 substrate for comparison. The line marked with an asterisk is a rotational Raman line of H_2 gas.

Stokes intensity. Even for the strong CaF_2 line no signal could be found for the anti-Stokes part.

Figure 7 shows the evolution with temperature of the peaks between 550 and 850 cm^{-1}. Obviously all lines are also present at room temperature, but they are rather broad and diffuse. With lower temperature they become sharper and sharper and more distinct. We conclude that no phase transformation occurs and produces new lines, but the linewidth decreases and the intensity increases.

D. Polarization resolved measurements

The polarization of the Raman lines has been analyzed both at room temperature and at 4 K. The results are displayed in Figs. 8 and 9. The lines which are visible in the perpendicular polarized spectra must have *E*-like symmetry. This is the case for the peaks Nos. 1, 8, 10, and 11. The

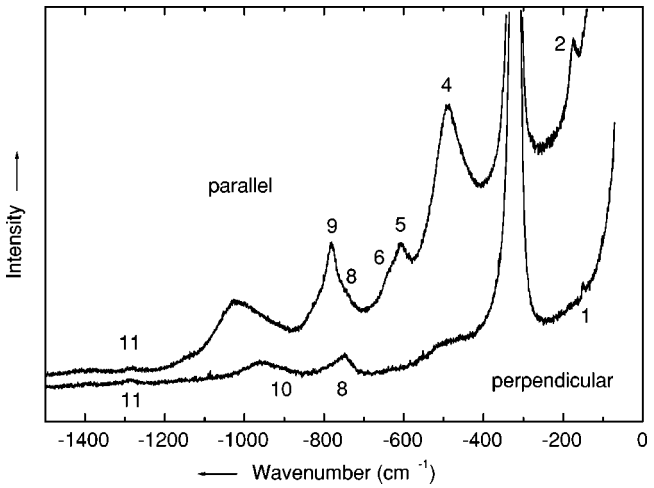

FIG. 8. Polarization resolved Raman spectra of an YH_3 film measured at an angle of incidence of 0° and a temperature of 300 K. The lines present in the perpendicular measurement belong to *E*-like phonons.

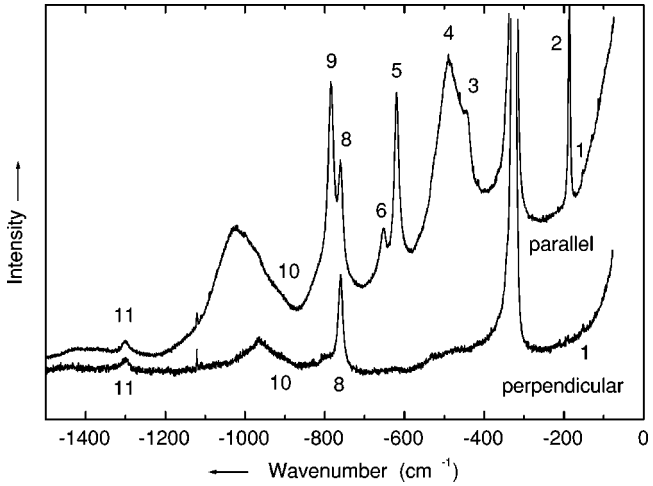

FIG. 9. Polarization resolved Raman spectra of an YH_3 film measured at an angle of incidence of 0 ° and a temperature of 4 K. The lines present in the perpendicular measurement belong to *E*-like phonons. Line No. 8 belongs possibly to another symmetry species than the other *E*-like phonons due to its narrow linewidth.

broad peak left to peak 10 is also present in a perpendicular polarized spectrum of a pure CaF_2 substrate. Because of the proximity of this big substrate line, the exact energy of peak 10 is difficult to determine. Therefore the error for the energy in Table VII is rather large. There is a remarkably large difference in the linewidth for the *E*-like phonons even in the low temperature measurements. Together with the comparison between Raman and IR spectroscopy (Sec. IV C) one can conclude, that the narrow line No. 8 belongs to a different symmetry species than the other *E*-like lines. The lines which appear only in the parallel configuration must have A_1 symmetry. The number of A_1 lines in our spectra is 6 and therefore too high for a $P\bar{3}c1$ structure (see Sec. II A). In a $P6_3cm$ or $P6_3$ structure we have 7 or 11 Raman active A_1 modes, which is compatible with the measurements.

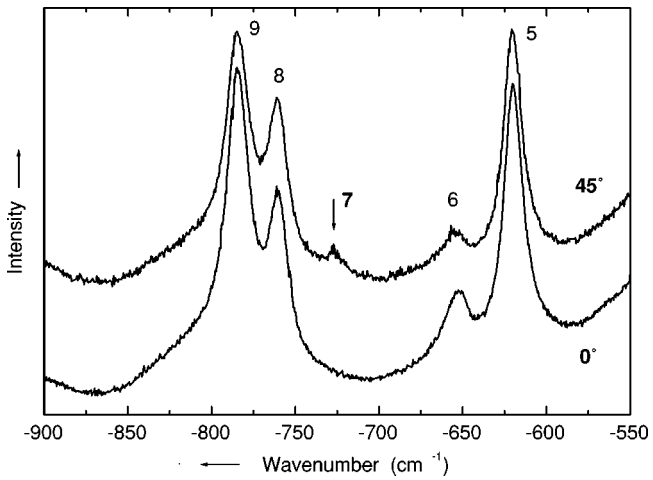

FIG. 10. Comparison of the Raman spectra of an YH_3 film measured at an angle of incidence of 0° and of 45° at 4 K. A new line (No. 7) appears at 45°.

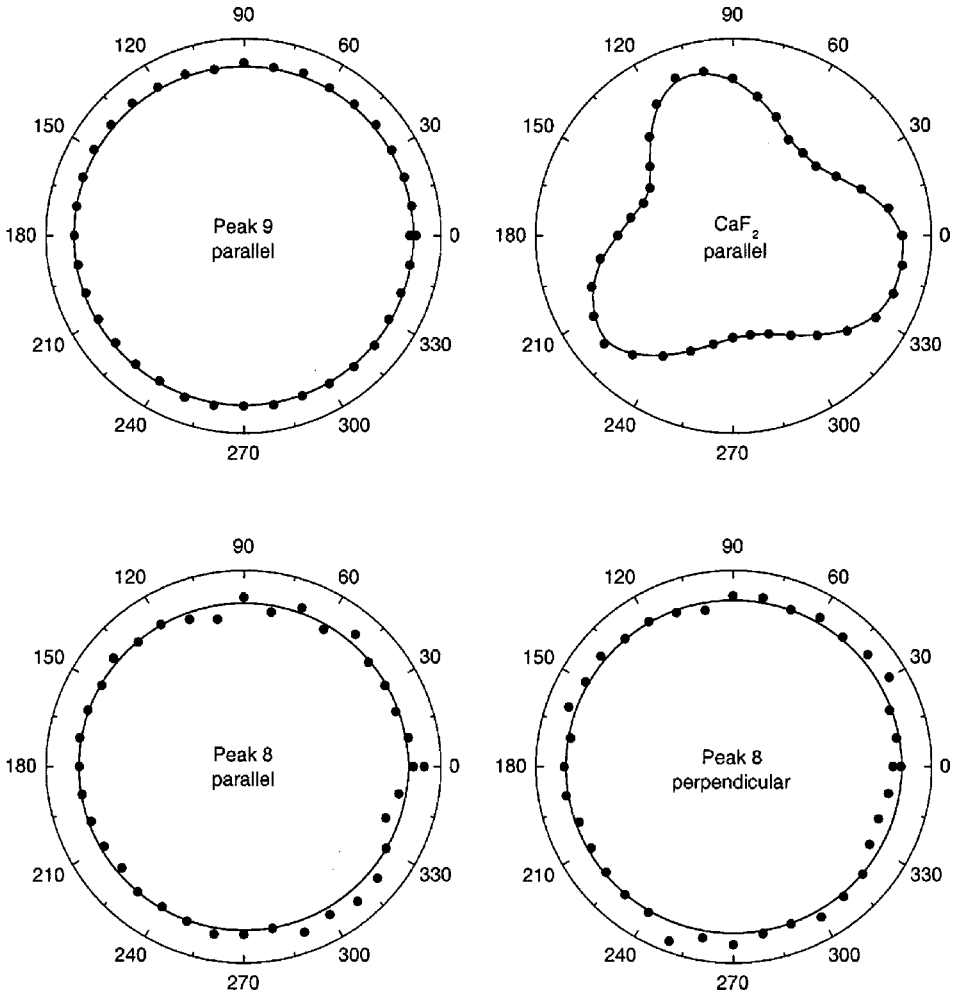

FIG. 11. Measured angular dependence of the intensity for two YH_3 peaks and the CaF_2 peak at room temperature. Peak 9 appears only for parallel polarization, whereas peak 8 appears in both polarization directions.

E. Different inclination angles

With polarization resolved measurements only at an inclination angle $\phi = 0°$ the question whether the *E*-like phonons have E_1, E_2, or E_g symmetry cannot be answered. Therefore measurements at an inclination angle $\phi = 45°$ have been performed. The result for the spectral range from 550 to 900 cm^{-1} at 4 K is shown in Fig. 10. A new Raman line appears when the direction of incidence is different from 0°. This is not possible if the crystal structure of YH_3 is $P\bar{3}c1$. This new line suggests a crystal structure such as $P6_3cm$ or $P6_3$, which has E_1 and E_2 phonons. Unfortunately clear changes of the intensities of the other *E*-like lines could not be found. Therefore from this measurement the doubly degenerated Raman lines can only be classified as being ''*E*-like.'' The only exception is the new line number 7, which has clearly the species E_1. The reason for the lack of clear changes in intensity might be the wide acceptance angle (35°) for the collected scattered light, which flattens the intensity profile for different inclination angles.

F. Angular dependence

For some Raman lines the angular dependence at an inclination angle $\phi = 45°$ was measured. With our experimental setup this was only possible at room temperature. The intensities were estimated from the spectra in a fit process with Lorentzians. The results are shown in Fig. 11 for the CaF_2 line, the strongest A_1 line at 784 cm^{-1} and the strongest *E*-like line at 751 cm^{-1}. For the *E*-like Raman line both polarization directions are shown. The measured angular dependence agrees very well with the characteristic shapes derived in Sec. II B for all displayed lines. The threefold symmetry of the pattern of the CaF_2 line is very distinct, only the minima are not as deep as calculated. This is due to the analyzer in front of the polychromator. Light can pass a polarizer even if its polarization is not parallel to the direction of the polarizer. The intensity decreases then proportional to $\cos^2 \vartheta$, if ϑ is the angle between the direction of the polarization and the direction of the polarizer. In this way especially the minima are partially filled with intensity from other angles. The shape for the A_1 phonon is nearly perfectly a circle, as calculated. In the case of the *E*-like phonon the deviations from the circular form are very small. It seems as if there are tiny indentations at the same angles as for the CaF_2 line, but they are the same both for parallel and perpendicular polarization. This cannot stem from an E_g phonon, because in this case they should appear on opposite sides for different polarizations. The origin of these features is more likely the proximity of the big CaF_2 line, which

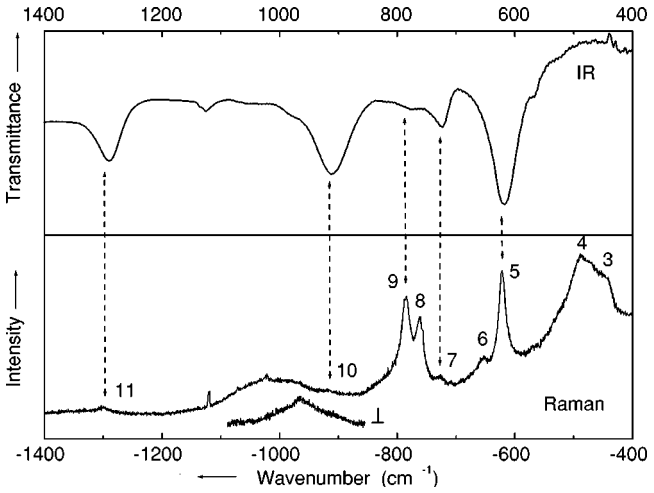

FIG. 12. Comparison of a Raman spectrum taken at 4 K and a FTIR spectrum measured at 77 K of an YH_3 film.

disturbs the fit processes of the small YH_3 lines with its angular dependence. Thus we conclude, that none of the special features for the angular dependence of the intensity of E_g phonons could be found.

G. Comparison with IR spectroscopy

From Sec. II A it is clear, that coincidence of lines in Raman and IR spectra should exist only if the crystal structure of YH_3 is noncentrosymmetric, i.e., it has the space group $P6_3cm$ or $P6_3$. However, only certain lines should appear, namely, those with A_1 or E_1 symmetry. Since the plane of atomic elongation for the E_1 phonons is the *ab* plane and the elongation direction for A_1 phonons is parallel to the *c*-axis, one can expect only small contributions from A_1 phonons in IR spectra. Therefore the E_1 phonons are more important for this comparison. IR spectra of YH_3 on GaAs substrates have been measured by Lee *et al.*[19] and also in our group.[24] Some of the lines observed in Ref. 19 are well known GaAs lines. Therefore IR transmission spectra of H-loaded Y films grown on Si (001) have been studied,[24] since Si has no IR active phonons in first order. The films are polycrystalline as in the case of films grown on GaAs.

In Fig. 12 a 77 K IR spectrum from a film grown on Si and a 4 K Raman spectrum for a film grown on CaF_2 are shown. There is obviously coincidence in the two spectra. The shift due to the different temperature is only about 10 cm^{-1} and is negligible compared to the big linewidth in the IR spectra. For the comparison one should keep in mind, that the phonon energy is not exactly at the minimum in the IR spectrum. The Raman lines 5, 7, 9, 10, and 11 agree very well with lines measured in the IR. The energies are again collected in Table VII. Most of the lines have *E* symmetry, except Nos. 5 and 9 which have A_1 symmetry. It is known that the growth of Y on GaAs and Si results in polycrystalline films. This might be a reason for the strong appearance of the *A*-like lines in the IR, although they should be small according to their direction of the atomic displacement. We conclude, that the structure of YH_3 must be noncentrosymmetric. Since in the $P6_3cm$ and $P6_3$ structure only the E_1 phonon modes are IR and Raman active, the line Nos. 7, 10, and 11 must have E_1 symmetry. Line No. 8 is also *E*-like, but not visible in the IR spectrum and should therefore have E_2 symmetry.

V. SUMMARY

We have reported measurements of the Raman effect in YH_3 and YD_3. Several lines have been found in the Raman spectra; they are rather broad and diffuse at room temperature but become very sharp and distinct at 4 K. Polarization resolved measurements in combination with a FGA and a calculation of the intensities in different scattering configurations reveal the symmetry species of the phonons. The number of experimentally observed A_1 phonons is not compatible with a $P\bar{3}c1$ structure. The appearance of new Raman lines for inclination angles different from 0° points towards a $P6_3cm$ or $P6_3$ structure of YH_3. According to our calculations the appearance of additional lines is not possible in a $P\bar{3}c1$ structure. Also in measurements of the angular dependence of doubly degenerated *E*-like phonon modes no indication for $P\bar{3}c1$ specific patterns was found. A comparison between Raman and IR spectra shows coincidence for several lines. Again this is possible only for a noncentrosymmetric structure such as $P6_3cm$ or $P6_3$ and not for $P\bar{3}c1$.

ACKNOWLEDGMENTS

The authors thank Thilo Lampe, Technische Universität Braunschweig, for technical support and Professor Roger Cowley, Clarendon Laboratory, Oxford, for helpful discussions. This work was financially supported by the European Commission through the TMR program (research network ''Switchable metal hydride films'').

*Electronic address: h.kierey@tu-bs.de; URL: http://www.tu-bs.de/institute/halbleiterphys/

[1] M. Kremers, N. J. Koeman, R. Griessen, P. H. L. Notten, R. Tolboom, P. J. Kelly, and P. A. Duine, Phys. Rev. B **57**, 4943 (1998).

[2] T. J. Udovic, Q. Huang, and J. J. Rush, in *Hydrogen in Semiconductors and Metals,* edited by N. H. Nickel, W. B. Jackson, and R. C. Bowman, MRS Symposia Proceedings No. 513 (Materials Research Society, Pittsburgh, 1998), p. 197.

[3] T. J. Udovic, Q. Huang, and J. J. Rush, J. Phys. Chem. Solids **57**, 423 (1995).

[4] T. J. Udovic, Q. Huang, R. W. Erwin, B. Hjörvarsson, and R. C. C. Ward, Phys. Rev. B **61**, 12 701 (2000).

[5] T. Udovic (private communications).

[6] P. J. Kelly, J. P. Dekker, and R. Stumpf, Phys. Rev. Lett. **78**, 1315 (1997).

[7] P. van Gelderen and P. J. Kelly (private communications).

[8] T. J. Udovic, Q. Huang, and J. J. Rush, Phys. Rev. Lett. **79**, 2920 (1997).

[9] G. Turrell, *Infrared and Raman Spectra of Crystals* (Academic

Press, London, 1972).
[10] H. Kuzmany, *Solid State Spectroscopy* (Springer Verlag, Berlin, 1989).
[11] A. P. Cracknell, *Applied Group Theory*, Selected Readings in Physics (Pergamon Press, Oxford, 1967).
[12] L. de Materiales de Universidad del País Vasco, *Bilbao crystallographic server*, URL http://www.cryst.ehu.es/cryst/
[13] R. T. Demers, S. Kong, M. V. Klein, R. Du, and C. P. Flynn, Phys. Rev. B **38**, 11 523 (1988).
[14] R. Loudon, Adv. Phys. **13**, 423 (1964).
[15] J. F. Nye, *Physical Properties of Crystals* (Oxford University Press, Oxford, London, 1957).
[16] D. G. Nagengast, J. W. J. Kerssemakers, A. T. M. van Gogh, B. Dam, and R. Griessen, Appl. Phys. Lett. **75**, 1724 (1999).
[17] A. Jacob, A. Borgschulte, and J. Schoenes, Verh. Dtsch. Phys. Ges. **35** (2000).
[18] N. I. of Standards and Technology, *NIST atomic spectra database*, URL http://physics.nist.gov/cgi-bin/AtData/main_asd
[19] M. W. Lee and W. P. Shin, J. Appl. Phys. **86**, 6798 (1999).
[20] J. Loader, *Basic Laser Raman Spectroscopy* (Heyden/Sadtler, London, 1970).
[21] X. Michaut, R. Saint-Loup, H. Berger, M. L. Dubernet, P. Joubert, and J. Bonamy, J. Chem. Phys. **109**, 951 (1998).
[22] T. J. Udovic, J. J. Rush, Q. Huang, and I. S. Anderson, J. Alloys Compd. **253–254**, 241 (1997).
[23] J. Schoenes, J. Hayoz, P. Aebi, and L. Schlapbach (unpublished).
[24] M. Rode, H. Kierey, A. Jacob, U. Barkow, A. Borgschulte, and J. Schoenes (unpublished).